

Implantable Multi-Cross-Linked Membrane-Ionogel Assembly for Reversible Non-Faradaic Neurostimulation

Joo Sung Kim, Junho Kim, Jun Woo Lim, Dong Jun Kim, Jong Ik Lee, Hanbin Choi, Hyukmin Kweon, Jiho Lee, Hyeono Yee, Ji Hong Kim, Bokyung Kim, Moon Sung Kang, Jae Hyun Jeong,* Sung-Min Park,* and Do Hwan Kim*



Cite This: *ACS Nano* 2023, 17, 14706–14717



Read Online

ACCESS |



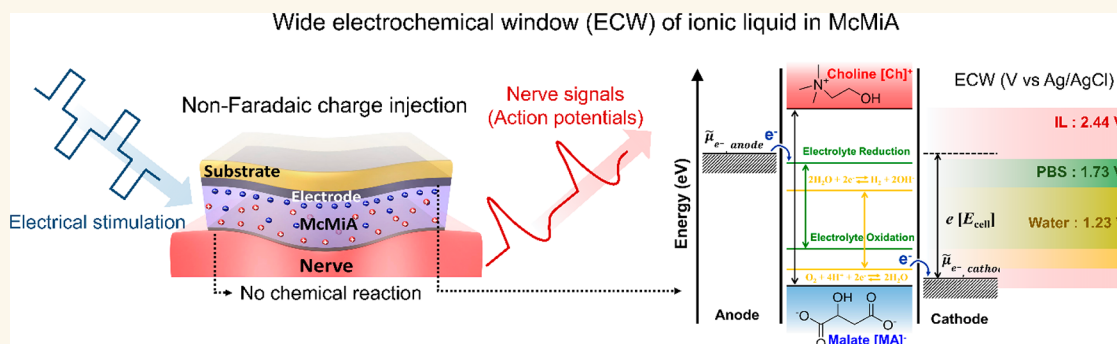
Metrics & More



Article Recommendations



Supporting Information



ABSTRACT: Neural interfaces play a major role in modulating neural signals for therapeutic purposes. To meet the demand of conformable neural interfaces for developing bioelectronic medicine, recent studies have focused on the performance of electrical neurostimulators employing soft conductors such as conducting polymers and electronic or ionic conductive hydrogels. However, faradaic charge injection at the interface of the electrode and nerve tissue causes irreversible gas evolution, oxidation of electrodes, and reduction of biological ions, thus causing undesired tissue damage and electrode degradation. Here we report a conformable neural interface engineering based on multicross-linked membrane-ionogel assembly (termed McMiA), which enables nonfaradaic neurostimulation without irreversible charge transfer reaction. The McMiA consists of a genipin-cross-linked biopolymeric ionogel coupled with a dopamine-cross-linked graphene oxide membrane to prevent ion exchange between biological and synthetic McMiA ions and to function as a bioadhesive forming covalent bonds with the target tissues. In addition, the demonstration of bioelectronic medicine via the McMiA-based neurostimulation of sciatic nerves shows the enhanced clinical utility in treating the overactive bladder syndrome. As the McMiA-based neural interface is soft, robust for bioadhesion, and stable in a physiological environment, it can offer significant advancement in biocompatibility and long-term operability for neural interface engineering.

KEYWORDS: conformable neural interface, soft conductors, multicross-linked membrane-ionogel assembly, overactive bladder syndrome, nonfaradaic neurostimulation

INTRODUCTION

Noncommunicable diseases have become the greatest challenge to global health, and many of these conditions are related to neurological disorders according to recent advances in neuro-engineering.^{1,2} Treatment and management technologies for these chronic conditions, therefore, focus on controlling the nervous system using artificial stimulation pulses based on electric, magnetic, optical, and ultrasound energy sources, which are called bioelectronic medicine. An

array of neurological disorders has been cured by traditional bioelectronic devices, including deep-brain stimulators,^{3,4}

Received: March 22, 2023

Accepted: July 24, 2023

Published: July 27, 2023



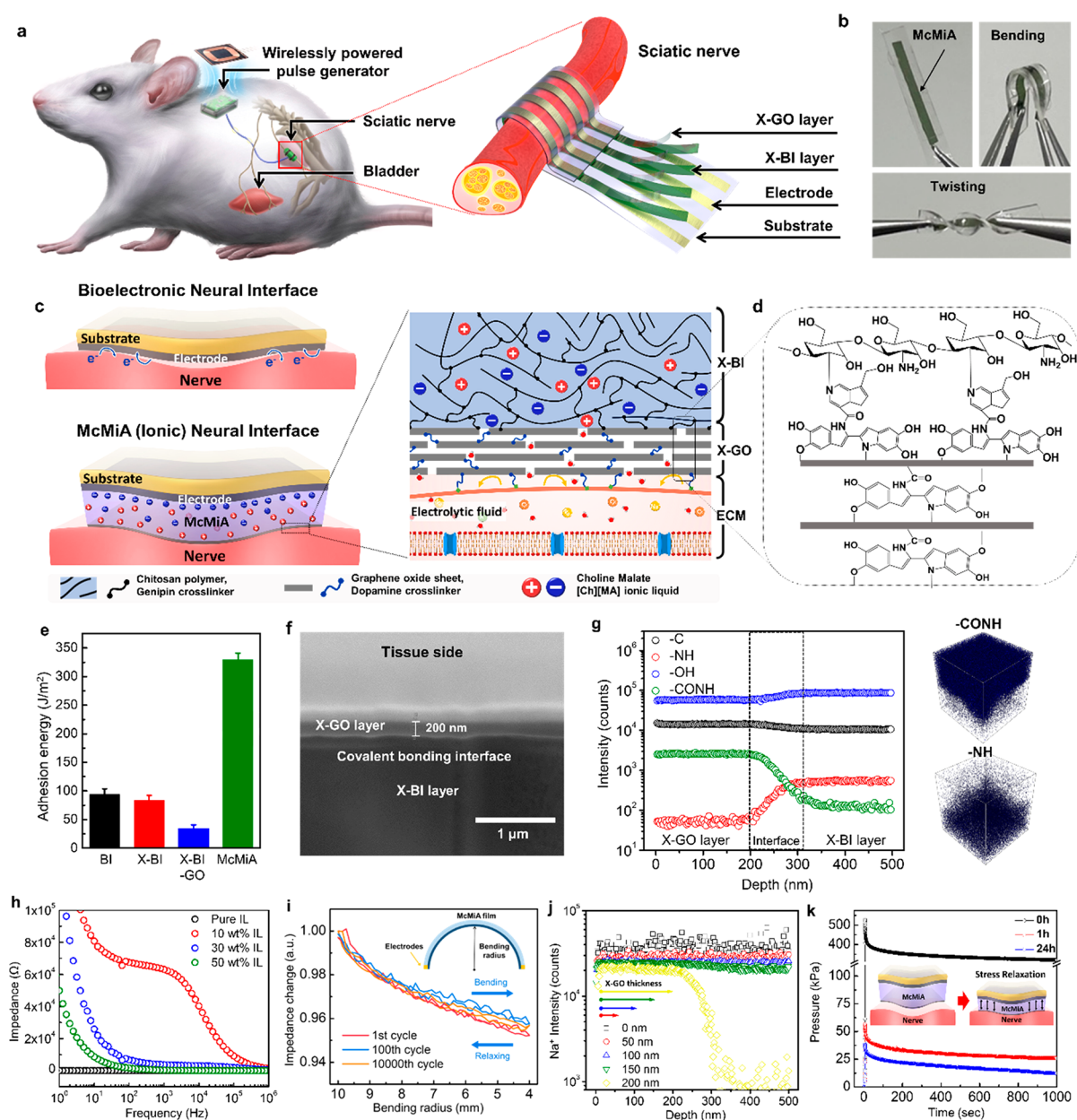


Figure 1. A multicross-linked membrane–ionogel assembly (McMiA) as a soft neural interface. (a) Schematics of the McMiA-based neural interface and neurostimulator device implanted in a rat to control overactive bladder syndrome. (b) Images of freestanding McMiA electrodes while being bent and twisted. (c) Material design of the McMiA-based neural interface. The McMiA comprises a dopamine-cross-linked graphene oxide (X-GO) membrane serving as an ion diffusion barrier and a genipin-cross-linked biopolymeric ionogel (X-BI) as a conductor. While conventional bioelectronic neural interfaces lead to mechanical and chemical mismatches, the McMiA-based neural interfaces enable bioelectronics for a stable and conformable contact without undesirable electrochemical reactions, such as water electrolysis, material oxidation, and ion reduction. (d) Molecular structure of X-GO layer containing dopamine and genipin cross-linkers covalent bond to chitosan polymer and GO layer, respectively. (e) Comparison of bioadhesive properties of X-BI, GO-coated X-BI, and the McMiA. (f) Cross-section FE-SEM image of focused ion beam (FIB)-etched region at the X-GO/X-BI interface of the McMiA film. (g) ToF-SIMS depth profiles of various species of interest acquired from the McMiA. (h) Impedance spectra of [Ch]⁺[MA]⁻ ionic liquid and X-BI as a function of ionic liquid concentrations (10–50% w/w). (i) Impedance change of the McMiA as a function of bending radius (10–4 mm) at different bending cycles (1, 1000, and 10,000). (j) ToF-SIMS depth profiles of Na⁺ ions of interest acquired from penetrated PBS into McMiA through X-GO membrane with different thickness (0–200 nm) after soaking in PBS for 24 h. (k) Time-dependent stress–relaxation behavior of the McMiA after soaking in PBS for 1–24 h.

spinal cord stimulators,^{5,6} and vagus nerve stimulators.⁷ While these stimulators directly stimulate the central nervous system or nerve bundles directly connected to the brain, recent studies on bioelectronic medicine have shifted to controlling organ functions by directly stimulating the organ or peripheral nerves connected to target organs.^{8,9} With the success of controlling

organ functions through peripheral nerve stimulation, the development of implantable miniaturized bioelectronic devices delivering stimuli to target peripheral nerves has been rapidly growing.¹⁰

Neural interfaces play a major role in modulating neural signals for therapeutic purposes. Representative neuromodula-

tion modalities include electrical and optogenetic techniques.^{11,12} Among these, optogenetic techniques have started gaining attraction due to their selectivity for specific nerves and the availability of biocompatible micro-sized light sources; however, the safety of opsins used in optogenetic techniques and their long-term stability still need to be proven. In this context, an electric neural interface using microelectrodes still possesses the greatest potential for miniaturized neural stimulators. For modern electric neurostimulation, platinum or iridium oxide metal electrodes^{13,14} are commonly utilized because of their low bulk resistance and high charge injection capability (CIC). However, these electrodes potentially cause undesirable contact between the solid metal and the soft tissues. These mechanical mismatches provoke tissue damage and interfacial defects, such as inconsistent tissue–electrode contact areas and cellular distances.¹⁵ As the electrode-induced electric field is heavily abated by the distance between the nerve and the electrodes, the cellular distance should be minimized, and the contact area must be maximized for the precise delivery of local field potentials into the targeted nerve.

Doped conducting polymers^{16–18} and hydrogels¹⁹ have been explored as soft electrode materials to develop promising neural interfaces without interfacial defects. Among these materials, poly(3,4-ethylenedioxythiophene):poly(styrenesulfonate) (PEDOT:PSS)-based soft hydrogels have attracted attention due to their favorable electronic conductivity, mechanical stretchability, and aqueous stability compared to molecularly doped conductive polymers. However, the electrolytic fluid in living systems (i.e., pH-buffering systems) can neutralize PEDOT:PSS hydrogels that are strongly acidic because of the presence of PSS. Thus, a physiological environment can also cause inconsistent conductivity of the PEDOT:PSS hydrogel, disturbing the π – π stacking of the PEDOT crystalline region.²⁰ More importantly, because the aqueous environment of extracellular media has a narrow electrochemical window (ECW), a direct interface with the electron-conducting materials, including graphene²¹ and carbon nanotubes (CNTs),²² causes a charge transfer reaction at neural interfaces. Such a faradaic charge injection mechanism can be detrimental to the long-term stability and biocompatibility of bioelectronics due to undesired gas evolution and electrode degradation caused by water electrolysis and electrode oxidation, respectively.²³ These chemical reactions during faradaic charge injection are typically irreversible due to the rapid diffusion of the gas. Moreover, ion species constituting solid-state electrolyte-based soft conductors (such as hydrogel electrolytes and ionogels) diffuse into the extracellular media owing to the concentration gradient and ion valency. The ion exchange that takes place at the neural interface, due to the diffusion of biological ions in extracellular media and synthetic ions in electrolyte-based conductors, can result in an electrolyte imbalance in the body. This imbalance has the potential to cause changes in blood pressure and disorders in the nervous system.²⁴

RESULTS AND DISCUSSION

Here, we report a conformable neural interface engineering based on biocompatible multicross-linked membrane–ionogel assembly (McMiA) soft electrodes for nonfaradaic neurostimulation of sciatic nerves to manage overactive bladder syndrome. Importantly, we incorporated a cross-linked graphene oxide (X-GO) membrane and a cross-linked biopolymeric ionogel (X-BI) conductor onto metal electrode-

coated flexible substrates to design the McMiA as a reliable neural interface, leading to the well-defined flexible characteristics of the McMiA (Figure 1a,b). The McMiA separates neural electrodes (conducting polymers or metal electrodes) from biological tissues by establishing a neural interface with a wider ECW than that of the electrolytic fluid in biological systems, which acts as an implantable neurostimulator to provide a nonfaradaic (capacitive) charge injection without undesirable electrochemical reactions such as water electrolysis, electrode oxidation, and biological ion reduction, even under high voltage; this was not the case with conventional faradaic neural interfaces (Figure 1c).

Material Design of McMiA. In this work, as a part of the McMiA, we introduced an X-BI conductor composed of choline-derived ionic liquids (ILs) and chitosan biopolymers to produce a capacitive current to the targeted nerve. Biocompatible choline malate ($[\text{Ch}]^+[\text{MA}]^-$) ILs, a component of most phospholipids in cell membranes,²⁵ were prepared by a neutralization reaction based on choline bicarbonate and malic acid (Supporting Information Figure S1 and supplementary text). The low melting point (-62.3°C) of $[\text{Ch}]^+[\text{MA}]^-$ is a critical property that enables ion conduction in a body temperature (37°C) environment (Figure S1d). Next, these $[\text{Ch}]^+[\text{MA}]^-$ ion pairs were blended with chitosan biopolymer to provide a biocompatible ionogel as an ionic conductor. Furthermore, we incorporated the X-GO membrane as the other part of the McMiA on the X-BI conductor surface to prevent ion exchange at the neural interface by addressing the tortuous diffusion pathway of stacked GO sheets.²⁶ Although both chitosan and GO membranes exhibit low cytotoxicity, they degrade via hydrolysis or enzyme-specific reaction of the chitosan chains and redispersion or swelling of the GO in an aqueous environment.²⁷ We addressed this issue by introducing genipin- and dopamine-based biocompatible cross-linkers into the chitosan-based BI conductor (Figures S2–S4 and supplementary text) and the GO membrane (Figures S4, S5 and supplementary text), respectively, for imparting bioadhesion properties as well as long-term reliability in the aqueous environment into the McMiA, while preserving the mechanical and electrical stability (Figure 1d). In particular, the McMiA functions as a bioadhesive forming covalent bonds with tissues (porcine skin) due to a reactive end group of the interlaminar dopamine (Figure 1e and Video S1).²⁸ In general, two cross-linkers of genipin and dopamine form a strong interface between the X-GO membrane and the X-BI conductor via the chemical Schiff base reaction (Figure S6), forming a stable layered structure of the McMiA, as shown in the cross-sectional field emission scanning electron microscope (FE-SEM) image (Figure 1f).

The time-of-flight secondary ion mass spectrometry (ToF-SIMS) data of McMiA demonstrated that the X-BI conductor exhibited a uniform distribution of genipin cross-linkers, represented by the amide groups shown in Figure 1g. Similarly, the X-GO membrane layer displayed a homogeneous distribution of dopamine cross-linkers, corresponding to the amine groups in Figure 1g. Moreover, the utilization of ToF-SIMS allowed us to obtain three-dimensional configuration data, enabling precise characterization of the uniform cross-linked state within a $100\ \mu\text{m} \times 100\ \mu\text{m}$ area, with a depth scale of 500 nm. In addition to the well-defined topology in the McMiA, the tissue-level ionic conductivity of the McMiA should deliver a reliable capacitive current. The bulk ionic

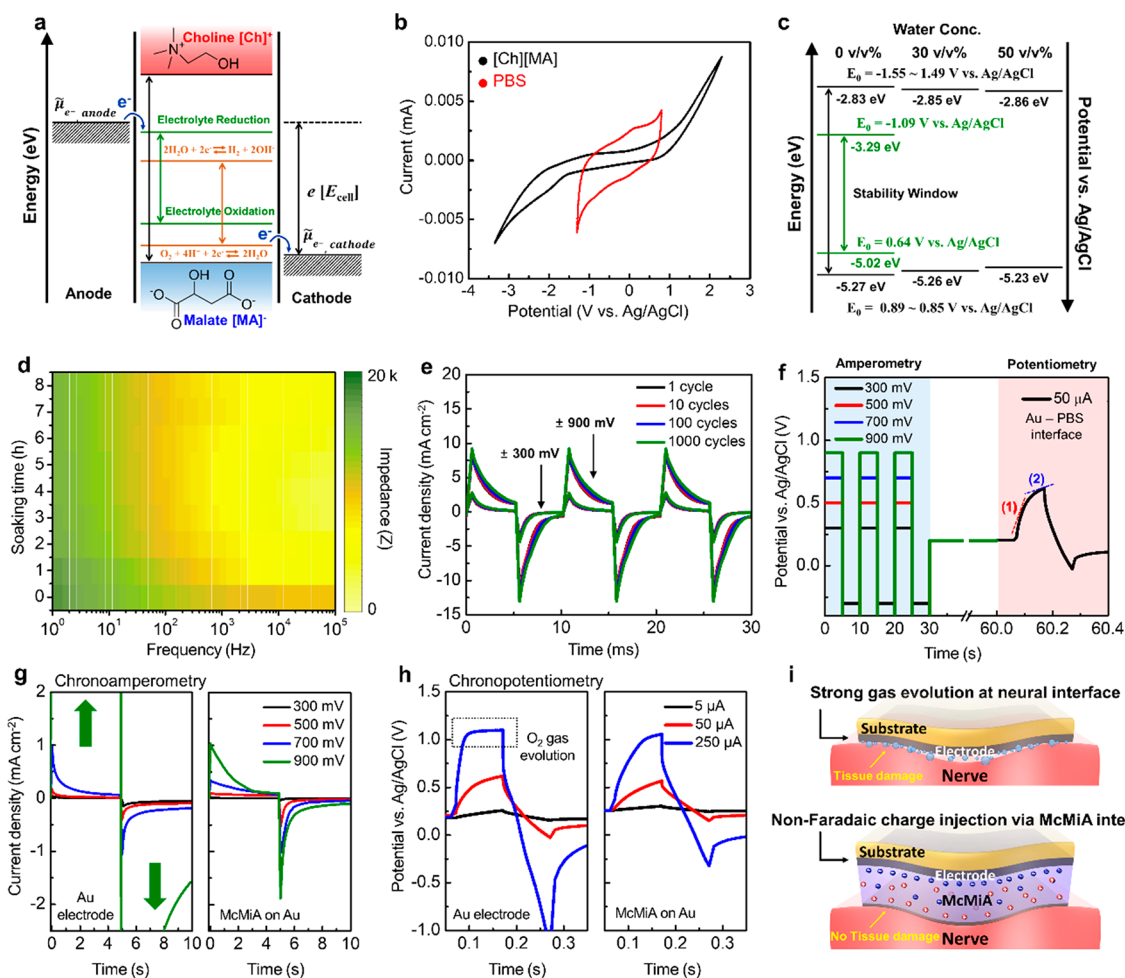


Figure 2. Electrochemical stability of the multicross-linked membrane-ionogel assembly (McMiA)-based neural interface in physiological-relevant environment. (a) Relative energy levels of the electrochemical window (ECW) for water hydrolysis, electrolyte solution (PBS), and $[\text{Ch}]^+[\text{MA}]^-$ ionic liquid. (b) Cyclic voltammograms of PBS and $[\text{Ch}]^+[\text{MA}]^-$ ionic liquid with a scan rate of 100 mV s^{-1} . (c) Thermodynamic potential and ECW of $[\text{Ch}]^+[\text{MA}]^-$ ionic liquids with different water concentration (0–50% v/v). (d) Impedance of the McMiA for 1–10,000 Hz after soaking in 0.1 M PBS for 1–8 h. (e) Charge injection curves of the McMiA at 1, 10, 100 and 1000 cycles. (f) Potential trace of chronocoulometry method for amperometry with different applied voltage biphasic pulses (300, 500, 700, and 900 mV) and potentiometric phase with constant current pulse ($50 \mu\text{A}$ for Au electrode). The slopes of the potential traces (1) and (2) correspond to eqs 1 and 2 in the text, respectively. (g) Current responses of Au electrode and the McMiA film on Au electrode in PBS under biphasic pulses (0.5–2 V). (h) Voltage responses of Au electrode and the McMiA film on Au electrode in PBS under current biphasic pulses (5, 50, and $250 \mu\text{A}$). (i) Schematic illustration of strong gas evolution at the neural interface between the common electrode and biological tissue and slight gas evolution at the McMiA interface between the McMiA film and biological tissue.

conductivity of the McMiA-based neural interface was 4 mS/cm after blending a maximum amount of $[\text{Ch}]^+[\text{MA}]^-$ (50% w/w) and preserving the solid-like property of McMiA, thereby showing a low impedance at physiologically relevant frequencies (10^2 to 10^5 Hz ; Figure 1h).²⁹ Moreover, the McMiA film showed stable impedance in a narrow bending radius (4 mm) similar to the sciatic nerve radius after 10,000 bending cycles (Figure 1i).³⁰ Notably, the ToF-SIMS data of the McMiA with 200 nm X-GO membrane revealed a significant reduction in the permeability of Na^+ ions even after 24 h of soaking in phosphate-buffered saline (PBS) solution, whereas the X-GO membranes with a thickness of 150 nm or less showed a consistent concentration of Na^+ ions in the X-GO and X-BI layers (Figure 1j and Supporting Information Figure S7).

In addition, the McMiA exhibited a low elastic modulus due to the plasticizing effect of ions (Figures S8, S9) but was also compressive-stress-free at the neural interface after being

soaked in PBS over 24 h because of its visco-poroelastic energy dissipation mechanism (Figure 1k). The chitosan polymer in the presence of water and the $[\text{Ch}]^+[\text{MA}]^-$ ILs, which reflects the mechanical behavior of the McMiA neural interface in a real aqueous environment, were viscoelastic and poroelastic deforming owing to polymer chain rearrangement and pore structure reconstruction, respectively.³¹ This visco-poroelastic behavior, a combination of these two effects, was further enhanced as the soaking time in PBS increased through the liquid flow-dependent poroelastic energy dissipation (Figures S10, S11).

Electrochemical Characterization of McMiA. Next, we investigated the electrochemical properties and stabilities of the McMiA film in a physiologically relevant environment, which is critical for stable nonfaradaic neurostimulation at the McMiA neural interface. This is because water electrolysis on oxygen evolution on the anodic side and hydrogen evolution on the cathodic side, defined by the so-called water window

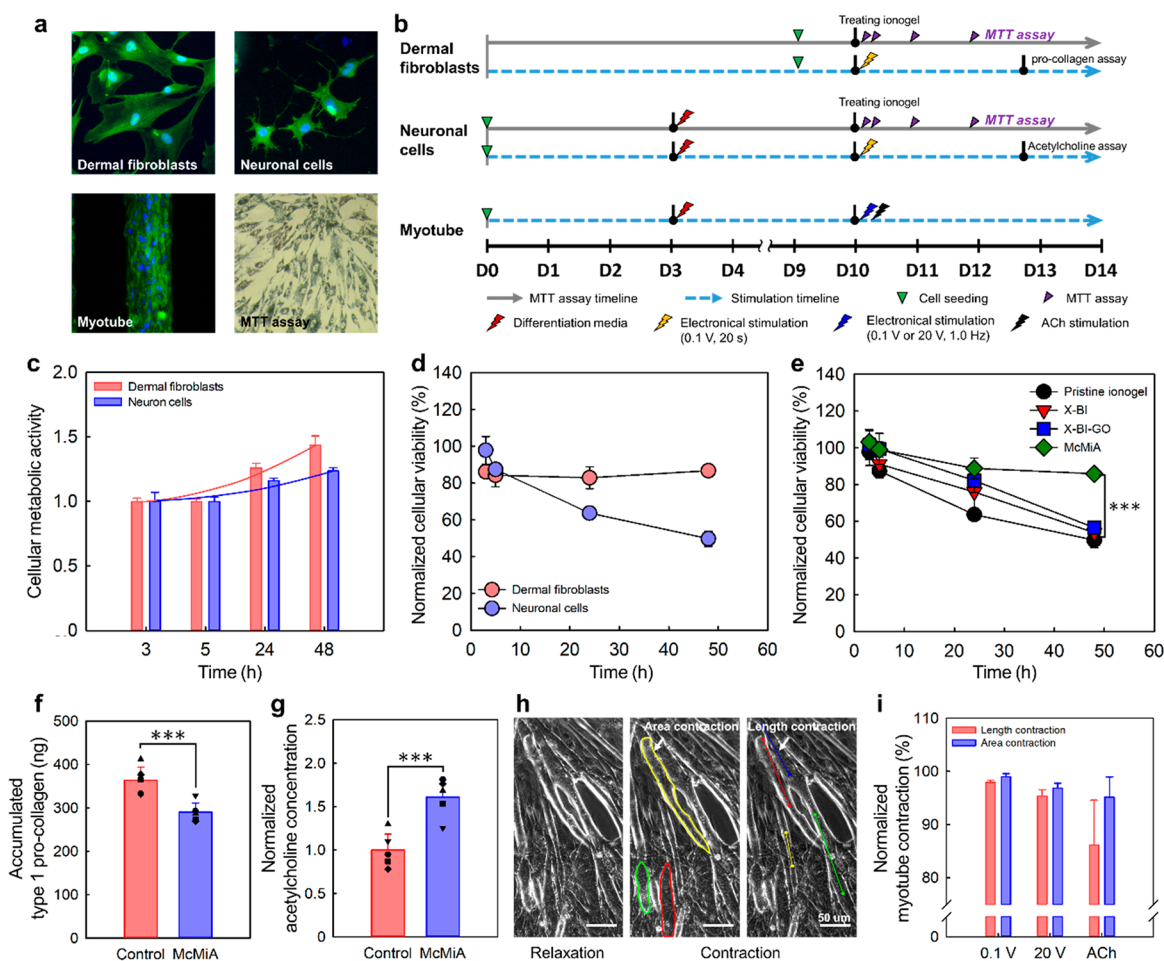


Figure 3. Cytotoxicity and physicochemical characterization of the multicross-linked membrane-ionogel assembly (McMiA). (a) Confocal images of dermal fibroblasts, neuronal cells, and myotubes and bright field images of 3-(4,5-dimethyl-2-thiazolyl)-2,5-diphenyl-2H-tetrazolium bromide (MTT) assay for cytotoxicity. (b) Timelines of MTT assay and stimulation for the cytotoxicity and physicochemical characterization. (c) Cellular metabolic activity of dermal fibroblasts and neuronal cells at each time point was normalized to the metabolic activity characterized right after cell stabilization on well. (d) The viability of pristine ionogel-treated dermal fibroblasts and neuronal cells at each time point was normalized to the characterized pure medium-grown cells. (e) The viability of pristine ionogel-, X-BI-, X-BI-GO-, and the McMiA-treated neuronal cells at each time point was normalized to the characterized pure medium-grown cells ($***p < 0.0005$). (f) The type I pro-collagen accumulated in electrically stimulated, pristine ionogel-treated, and McMiA-treated dermal fibroblasts after 72 h. (g) The acetylcholine (ACh) concentration in electrically stimulated, nontreated, and McMiA-treated neuronal cells after 72 h. (h) The bright field images and analysis of relaxation and contraction of ACh-stimulated myotubes. (i) Effects of electrical and ACh stimulation on myotube stimulated with electric potential raised to ± 0.1 and ± 20 V and ACh obtained in neuronal cells 72 h after electrical stimulation.

(1.23 V for pure water), is an irreversible process that lowers biocompatibility in biological applications (Figure 2a).³² In this regard, the ECW and voltage pulse ranges in the neural interface should be widened. To this end, we synthesized $[\text{Ch}]^+[\text{MA}]^-$ ILs that can exhibit a broad ECW (2.44 V measured using cyclic voltammograms [CVs]), whereas 0.1 M PBS solution showed a narrow ECW (1.73 V; Figure 2b and Figure S12). The cathodic and anodic limited potentials were determined by $[\text{Ch}]^+$ reduction to trimethylamine and $[\text{MA}]^-$ oxidation to oxaloacetate. Importantly, the ECW did not decrease significantly until the water content reached 50% (w/w), as indicated by the swelling ratio of McMiA (Figure 2c and Supporting Information Figure S13). This phenomenon can be attributed to the higher concentration of “bound water”, which includes the hydrophilic $[\text{Ch}]^+[\text{MA}]^-$ ions and water molecules, compared to the “free water” adsorbed at the electrode surface. This higher concentration of bound water helps to mitigate water electrolysis.^{33,34} In addition, the

McMiA swelling in an aqueous environment decreased with the viscosity of $[\text{Ch}]^+[\text{MA}]^-$ and enhanced the ionic conductivity, owing to water-mediated ion pair dissociation. The complex impedance of the McMiA was decreased by more than three times from 1742 to 541 Ω (100 Hz) while incubating for 3 h in 0.1 M PBS solution at 37 $^\circ\text{C}$ and then stabilized (Figure 2d and Figure S14).

We also characterized the CIC of the McMiA-based neural interface under various operating conditions to assess its impact on the electrical stimulation efficacy of neurostimulators (Figure 2e). The CIC of the McMiA were ~ 10 and ~ 50 $\mu\text{C cm}^{-2}$ with 300 and 900 mV biphasic pulses, respectively, which are comparable to those of pristine metallic electrodes (Figure 2e). Moreover, we evaluated the electrochemical stability of McMiA using cyclic CIC measurements under various biphasic pulses (300–900 mV). It should be noted that the McMiA exhibited consistent CIC values even after 1000 charging and discharging cycles (Figure 2e). This

consistency in the CIC values is due to the absence of unfavorable faradaic charge injection, such as water electrolysis, in the PBS. While conventional neurostimulation is commonly demonstrated using only the potential difference between two electrodes without a reference electrode, we systematically used chronoamperometry and chronopotentiometry to compare the differences in electric potential and current responses between faradaic charge injection of the metallic electrode and nonfaradaic (capacitive) charge injection of the McMiA-based neural interface (Figure 2f). In the chronoamperometric studies (potential-controlled method), different voltage amplitudes (300–900 mV vs Ag/AgCl) were specified, which can cause gas evolution (Figure 2g, left).³⁵ Therefore, in the water window region (700–900 mV vs Ag/AgCl), a small potential change strongly increases the faradaic currents for the Au electrode. However, it was observed that the anodic and cathodic currents did not show a significant increase at the Au electrode/McMiA interface. This can be attributed to the formation of an electric double layer (EDL) consisting of under 900 mV biphasic voltage pulses (Figure 2g, right).

In the chronopotentiometric studies (current-controlled method), the potential increased steeply upon anodic polarization as the current passed through the electrolyte resistance (R_i), causing an iR_i voltage drop, and then increased steadily after EDL formation.³⁶ The double-layer charging (capacitive) current can be expressed as

$$I = C_d \, dV/dt \quad (1)$$

where C_d is the EDL capacitance. If there is a sufficient increase in the electrode potential (~ 1 V), faradaic reactions occur, saturating the majority of the current. The faradaic current can be expressed as

$$I = e^{(nF(V-V_0)/RT)} \quad (2)$$

No plateau regions were observed in the voltage response for the Au electrode/McMiA interface, even under a 250 μ A biphasic current pulse (Figure 2h). However, the anodic potential quickly flattens at the Au electrode/PBS interface, indicating irreversible faradaic reactions with substantial oxygen evolution (Figure 2i). Consequently, the ECW should be expanded through the McMiA-based neural interface to prevent undesirable gas evolution, particularly when a high voltage/current is required.

Cytotoxicity and Physicochemical Characterization of McMiA. Next, we evaluated the *in vitro* biocompatibility of the McMiA-based neural interface using dermal fibroblasts and neuronal cells (Figure S15). In particular, neuronal cells were differentiated from the neuronal cell line PC12 and successfully induced neurite growth (Figure 3a and Figure S16a). The cells (2.0×10^4 cells/cm²) were cultured with various submerged ionogels (1.5 mg; Pristine, X-BI, X-BI-GO, and McMiA) in 96-well plates for 48 h. Cell viability was quantitatively evaluated using the 3-(4,5-dimethyl-2-thiazolyl)-2,5-diphenyl-2H-tetrazolium bromide (MTT) assay (Figure 3b). The optical density (OD) measurements at 3, 5, 24, and 48 h after these assays were converted to relative cell viability (%) by normalizing to 3 h (Figure 3c) and the control (Figure 3d,e).

First, the cytotoxicity of the dermal fibroblasts and neuronal cells was measured by using a pristine ionogel with $[\text{Ch}]^+[\text{MA}]^-$ ion pairs. The viability of dermal fibroblasts remained statistically constant for 48 h (approximately 85%). However, the viability of neuronal cells decreased to $98 \pm 7.5\%$, $64 \pm 3.1\%$, and $50 \pm 4.2\%$ after 3, 6, and 48 h,

respectively (Figure 3d). This result indicates that the $[\text{Ch}]^+[\text{MA}]^-$ ILs in the pristine ionogel are more cytotoxic to neuronal cells than to fibroblasts. In addition, the viability of neuronal cells after using X-BI, X-BI-GO, and McMiA for 48 h were $54 \pm 5.3\%$, $56 \pm 1.3\%$, and $86 \pm 2.8\%$, respectively (Figure 3e). Thus, the cytotoxicities of X-BI and X-BI-GO were similar to that of pristine ionogel, whereas the McMiA had low cytotoxicity. Both McMiA and X-BI-GO are based on GO membranes. However, McMiA incorporates cross-linked GO with dopamine, while X-BI-GO does not have cross-linking in the GO membrane. This difference results in a reduced mechanical stability for X-BI-GO, leading to swelling and delamination in solution. As a result, X-BI-GO exhibits similar low cytotoxicity to X-BI. On the other hand, it was observed that McMiA, with its cross-linked GO membrane, demonstrated enhanced cell survival ability due to the ionic diffusion barrier effect. Based on the cellular viability analysis, the major function of the X-GO membrane in blocking the $[\text{Ch}]^+[\text{MA}]^-$ diffusion from the X-BI in the absence of stimulation was validated.

In addition, the amount of type I pro-collagen secreted in electrically stimulated dermal fibroblasts (HDFn) was analyzed to confirm the ion diffusion barrier effect of the McMiA.^{37,38} To assess the impact of ion diffusion on cells within the extracellular matrix, we administered electrical stimulation using two types of electrodes: a pristine ionogel-based electrode as a control and a McMiA-based electrode. The HDFn cells (1.0×10^5 cells/mL) were cultured in 12-well transwells, electrically stimulated at 1.0 V for 20 s through a 1.2 mm electrode with and without the McMiA, and then incubated for 72 h after stimulation (Figure S17a). Cellular metabolic activity was quantitatively assessed using a type I pro-collagen immunoassay. The OD measurements at 12, 24, 48, and 72 h were converted to accumulated type I pro-collagen (ng). The amount of type I pro-collagen observed at 72 h in HDFn cells directly stimulated through the pristine ionogel increased by 25% compared to HDFn cells stimulated with McMiA (Figure 3f and Figure S17b,c). This suggests that the stimulation provided by the pristine ionogel, which allows for ion diffusion through the $[\text{Ch}]^+[\text{MA}]^-$ ions, resulted in increased cellular synthesis and secretion, in contrast to the stimulation provided by McMiA, which effectively blocks ion diffusion. Furthermore, in conjunction with the cellular viability results, electrical stimulation through McMiA demonstrates the ability to provide electrical stimulation without cellular toxicity independent of the influence of ion diffusion through an ion barrier effect. Then, acetylcholine (ACh) production was analyzed to evaluate the effect of electrical stimulation of the neurons using McMiA. To validate the alterations in the ACh production caused by electrical stimulation, we designated the group without electrical stimulation as the control group and compared it with the nerve cells that were electrically stimulated using McMiA. Cell concentration, electrode size, and stimulation conditions were identical to those of the evaluation using the HDFn. PC12 cells were successfully differentiated into neuronal cells in 12-well transwells and stimulated electrically. Additionally, C2C12 cells were differentiated into myotubes for evaluation of contraction to ACh (Figure S16b). We note that the McMiA-stimulated neuronal cells secreted 1.6-fold more ACh after 72 h than the unstimulated neuronal cells (Figure 3g and Figure S17d,e). These findings suggest that electrical stimulation through McMiA enhances the ACh secretion in neuronal cells,

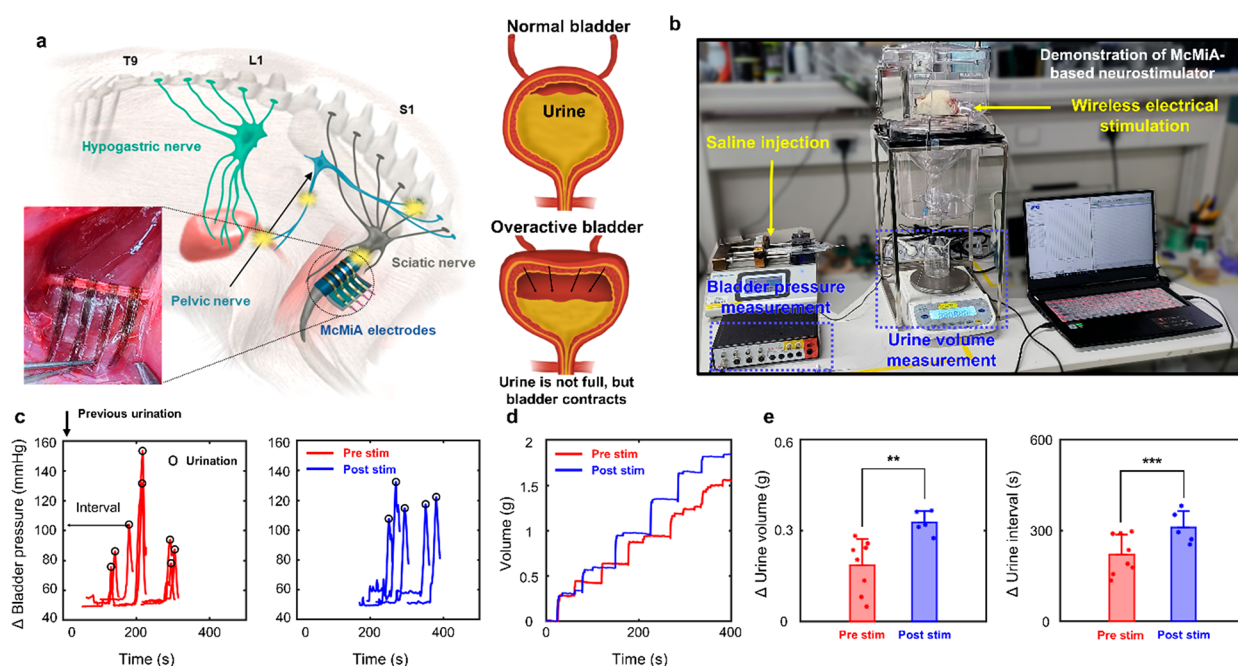


Figure 4. *In vivo* neural stimulation, experiment results, and data analysis. (a) Schematic diagram of the bladder nervous system. Sympathetic fibers (hypogastric nerves) originated the T11 ~ L2 segment of the spinal cord, and parasympathetic fibers (pelvic nerves) originated the S2 ~ S4 segment of the spinal cord. A normal bladder urinates when it is full, but an overactive bladder causes muscle contractions to expel urine even when the bladder is not full. (b) Experimental setting for measuring bladder pressure and urine volume while continuously injecting saline into the bladder of a rat. (c) A graph expressing the bladder pressure at each urination according to the time difference from the previous urination. (d) The comparison of cumulative urine volume before and after neurostimulation. (e) Analysis of urine volume and urination interval showing urination activity (bar: mean \pm SD).

which is consistent with previous studies demonstrating the release of the ACh in response to electrical stimulation in peripheral nerves.³⁹ Then, myotubes were treated with culture medium containing ACh produced from the McMiA-stimulated neuronal cells after 72 h, which contracted (Figure 3h and Video S2). The analysis of contraction was measured as the length of intracellular organelles and the area of the myotube and normalized to the length and area of the relaxed myotube. In addition, the degree of contraction was normalized based on the state of myotubes before stimulation. Myotubes stimulated by electrical stimulation contracted 2.1% and 4.6% in length and 1.0% and 3.1% in area at voltages of 0.1 and 20 V and frequency of 1.0 Hz. In addition, myotubes stimulated for 30 min with a culture medium containing acetylcholine contracted about 13.9% in length and 4.8% in area (Figure 3i). This indicates that the electrical potential stimulated the neuronal cells to increase production and secretion of the neurotransmitter ACh, which in turn stimulated skeletal muscle contraction.

Evaluating Effectiveness of Neurostimulator for Overactive Bladder: In Vivo Experiments and Data Analysis. With the *in vitro* biocompatibility and efficient physicochemical characterization of McMiA, we used the McMiA-based neurostimulator for *in vivo* experiments. Before integrating the device, a simple experiment was conducted to verify the effectiveness of electrical stimulation generated from the proposed neurostimulator. A valid way to confirm sciatic nerve stimulation is to confirm the leg tremor, as a biological response of the sciatic nerve to the electrical stimulation. After hair removal on the thigh, the skin and muscles were incised to expose the sciatic nerve. The prepared electrode was connected to the nerve, and electrical stimulation generated

from the proposed device was applied. The effectiveness of the proposed stimulator system was clearly confirmed by observing leg tremors (Video S3). In general, overactive bladder (OAB) syndrome refers to a group of symptoms related to sudden bladder contraction even when it is not full, causing frequent and sudden urination that is difficult to control. Urination is caused by detrusor muscle contraction controlled by neural signals transmitted through a large neural network between the lower urinary tract and spinal cord.⁴⁰ The lower urinary tract is innervated by the peripheral nerves associated with the parasympathetic (pelvic nerves) and sympathetic (hypogastric nerves and sympathetic chain) originating from L2–S4 of the spinal cord (Figure 4a).⁴¹ By artificial stimulation of a nerve branch in this complex neural network related to bladder activity, micturition can be controlled to mitigate these symptoms. Currently, the clinically accepted neuromodulation techniques used as second-line treatments for bowel incontinence include sacral nerve stimulation (SNS) and percutaneous tibial nerve stimulation (PTNS).⁴² Although both SNS and PTNS have few side effects and proved effectiveness for OAB, PTNS is a relatively simple, less invasive, and cost-effective method because it requires surgical revision.^{43–45} As the tibial nerve is a distal branch of the sciatic nerve composed of fibers from L4 to S3, the effect of stimulating afferent fibers of the tibial nerve can be achieved by stimulating the sciatic nerve.⁴⁶ Due to the ease of electrode implantation and accessibility, we observed changes in urination activity while stimulating the sciatic nerve to demonstrate the effectiveness of the McMiA-based neurostimulator (Figure S18). Urination interval and amount were used as representative biomarkers for confirming urination suppression. Since bladder pressure measurement can be noisy

due to other factors, such as movement, urine activity can be distinguished only when the amount of urine and changes in bladder pressure are measured simultaneously (Figure S19).

Figure 4b shows the experimental setting for measuring the amount of urine and bladder pressure before and after the stimulation session. Saline was continuously injected through a tube connected to the bladder of the rat using a syringe pump (Legato 210P, KD Scientific). Urine was collected under the cage, and the amount of urination was measured while simultaneously measuring the bladder pressure in the absence of stimulation. Nerve stimulation was then applied, and the same measurements were taken. To analyze the effect of stimulation on micturition, bladder pressure waveforms at the moment of urination were extracted and plotted based on the immediately preceding urination time, representing the interval between each urination (Figure 4c). The red and blue lines, respectively, represent before and after stimulation, and Figure 4d shows the accumulated urine volume. Figure 4e illustrates the differences in the volume of urine per void and the urination intervals before and after stimulation. The mean volume of urine per voiding was 0.1865 ± 0.0867 g (mean \pm SD) before stimulation. Following stimulation, the voiding volume was 0.3272 ± 0.0376 g, resulting in an approximately 75% increase in the volume of urine per voiding ($p < 0.01$). The urination interval was 222 ± 65.5 s before stimulation and 311.2 ± 54.3 s after stimulation, representing an approximately 35% increase in the urination interval ($p < 0.05$). The mean peak bladder pressure before and after stimulation was 101.3 ± 27.6 and 118.8 ± 9.2 mmHg, respectively, with a 17% increase ($p = 0.2021$). From these results, it can be inferred that our proposed McMiA-mediated neural stimulation system effectively suppressed urination.

CONCLUSIONS

In summary, we demonstrated a fully biocompatible McMiA-based neurostimulator to achieve a nonfaradaic, conformable neural interface for wet tissues. Along with the stress-free and bioadhesive capabilities, nonfaradaic charge injection of the McMiA-based neural interface enables highly stable neurostimulation without any charge transfer reaction and irreversible tissue damage. In addition, systematically validated *in vitro* electrochemical analysis (such as chronoamperometry and chronopotentiometry) of the McMiA provides valuable insights for developing neurostimulators with enhanced electrochemical stability in a physiological environment. The McMiA integration with wireless neurostimulators has proven its preclinical efficacy as an implantable bioelectronic medicine for treating overactive bladder syndrome. Consequently, the McMiA-based neural interface not only provides a promising solution to address the mechanical and chemical mismatches at the electrode–electrolyte interface of bioelectronics but also facilitates the easy expansion of the ECW for fully reversible nonfaradaic neurostimulation.

EXPERIMENTAL SECTION

Synthesis of Biocompatible $[\text{Ch}]^+[\text{MA}]^-$ ILs. Biocompatible ILs ($[\text{Ch}]^+[\text{MA}]^-$) were synthesized via salt metathesis. Malic acid was dissolved in methanol (2 M) and slowly added to 0.8 M choline bicarbonate (Sigma-Aldrich; St. Louis, MO, USA) with mild stirring at 25 °C for 4 h to remove carbon dioxide generated by the reaction. Methanol and water in the mixture were eliminated by rotary evaporation at 80 °C for 2 h and subsequently dried in a vacuum oven at 80 °C for 48 h.

The synthesized $[\text{Ch}]^+[\text{MA}]^-$ was characterized through Fourier transform infrared spectroscopy (Bruker Optics GmbH (Germany) spectrometer) conducted in the attenuated total reflection (ATR) mode (ZnSe crystal). Each spectrum, recorded as the average of 64 scans with 2 cm^{-1} resolution, was collected from 4000 to 450 cm^{-1} . To verify the chemical structure of $[\text{Ch}]^+[\text{MA}]^-$, nuclear magnetic resonance (^1H NMR) spectroscopy (AvanceIII-500, Bruker) was performed by using a 500 MHz NMR spectrometer. To prepare the samples, $[\text{Ch}]^+[\text{MA}]^-$ was dissolved in an NMR solvent (deuterated dimethyl sulfoxide, DMSO- d_6). Chemical shifts are given in ppm, with residual solvent signals as an internal standard. Differential scanning calorimetry (DSC, DSC-Q20, TA Instruments) was also performed to confirm the melting point of $[\text{Ch}]^+[\text{MA}]^-$ under a N_2 atmosphere over two complete scans from -80 to $150\text{ }^\circ\text{C}$.

McMiA Fabrication. The McMiA film was prepared in three main steps: (i) $[\text{Ch}]^+[\text{MA}]^-$ -based X-BI solution preparation, (ii) X-GO membrane preparation, and (iii) McMiA film preparation. In the first step, a chitosan polymer solution was prepared by mixing a chitosan solution, which included 2% (w/w) chitosan (medium molecular weight, Sigma-Aldrich, Saint Louis, MO, USA) in 1% (v/v) acetic acid. Depending on the IL concentration (10, 30, 50% w/w), $[\text{Ch}]^+[\text{MA}]^-$ was mixed with the chitosan solution for 24 h at room temperature and dispersed into a genipin solution containing 50% DI water for cross-linking.

In the second step, the X-BI solution was poured into the polydimethylsiloxane (PDMS) mold substrate and cured for 48 h at room temperature. In the last step, tris(hydroxymethyl)-aminomethane was dissolved in a GO solution (GO-V20, 0.5% w/w in deionized water, Standard Graphene, Korea) followed by adjusting the pH to 8.5 by addition of 1 M HCl solution. Dopamine (Sigma-Aldrich, St. Louis, MO, USA) was added to the GO solution under vortexing at room temperature to obtain the X-GO solution. X-GO membrane was fabricated by spray coating on the X-BI film with an X-GO solution at 100 °C to remove the solvent. The completed McMiA was subjected to a soaking time of more than 3 h in PBS to achieve a swollen state prior to conducting *in vivo* experiments. This mold-assisted drying/swelling process limits in-plane isotropic swelling, thereby mitigating the occurrence of cracks and delamination within the X-GO membrane (Figure S20).

ToF-SIMS Analysis. The distributions of genipin and dopamine and their possible interactions were investigated by time-of-flight secondary ion mass spectrometry (ToF-SIMS, ToF SIMS-5, ION-TOF, Germany). Negative and positive ion spectra were obtained using an $\text{Ar}1000^+$ beam (2.5 keV) to etch the sample and a Bi^{3+} beam (30 keV) to analyze the given sample area ($100\text{ }\mu\text{m} \times 100\text{ }\mu\text{m}$).

Mechanical Characterization of McMiA. The tensile tests of pristine Chitosan and X-BI films were conducted using a DMA 850 instrument (TA Instruments) with dimensions of $1.5 \times 0.5\text{ cm}$ and a thickness of 0.1 cm. The tensile load was applied to the specimens, until the samples were broken. The surface modulus was obtained via Derjaguin-Muller-Toporov (DMT) model-based nanomechanical analysis mode of AFM (Park System, NX10) with a probe from Park System (SD-R30-CONT, resonant frequency $\approx 13\text{ kHz}$, $k \approx 0.2\text{ N/m}$, tip radius $\approx 30\text{ nm}$). The stress-relaxation response for viscoporoelastic behavior was measured using a custom-built testing machine connected with a precision force gauge (Mark-10). McMiA film with thickness of $200\text{ }\mu\text{m}$ was cut into rectangles with an area of $0.5\text{ cm} \times 0.5\text{ cm}$. After the application of an instantaneous step strain of 15%, the pressure applied to the film was monitored for 1000 s.

Electrochemical Characterization of McMiA. CV measurements were carried out without using supporting electrolytes or solvents. Before analysis, the solution was vigorously bubbled through dry argon for 25 min. All CV curves were obtained at a scan rate of 100 mV/s . A glassy carbon electrode was used as the working electrode, and a Pt coil electrode was used as the counter electrode with the Ag/AgCl reference electrode. After mixing with water, the solution was vigorously mixed and degassed with dry argon for 20 min. To determine the ion conductivity and CIC, electrochemical impedance spectroscopy (EIS), chronoamperometry, and chronopotentiometry were performed using an electrochemical analyzer

(PFSTAT302N, Metrohm Autolab). EIS was conducted at room temperature from 1 Hz to 100 kHz with a 10 mV AC signal. The KP solid cell (Wellcos Corp., Korea) was used for EIS under different McMiA film conditions. The ionic conductivity (σ) was calculated using the following equation. ($\sigma = R^{-1}A^{-1}L$, where R , A , and L are the resistance, area, and thickness of the film, respectively).

Swelling Test. The swelling experiment was conducted by soaking the films in a PBS buffer containing 1.5 $\mu\text{g/mL}$ of Lysozyme (Lysozyme from chicken egg white, Sigma-Aldrich) at 37 $^{\circ}\text{C}$ for 24 h. After swelling, the films were placed on filter paper to remove excess water, and their swollen weights (W_s) were measured. Subsequently, the films were dried in a vacuum oven for 48 h, and their dry weights (W_d) were measured. The swelling ratio was calculated using the following equation: Swelling ratio: $(W_s - W_d)/W_d$.

Culture of Dermal Fibroblasts, Neurons, and Skeletal Muscle Cells. Neonatal human dermal fibroblast cells (HDFn, Gibco; NY, USA) were cultured in a growth medium consisting of human fibroblast expansion medium (M106, Gibco), low-serum growth supplement (LSGS, Gibco), and 1% penicillin–streptomycin (P/S, 100 \times , Biowest; MA, USA) in a 75 cm^2 culture flask. After culturing until more than 80% confluence, the cells were plated at low density (1×10^4 cells/ cm^2) in a 96-well plate for MTT assay. A neuronal cell line (PC12, ATCC, USA) was cultured in a growth medium consisting of RPMI1640 (Gibco), 10% horse serum (HS, Biowest), 5% fetal bovine serum (FBS, Biowest), and 1% P/S (100 \times , Biowest) in a 75 cm^2 culture flask. After culturing to allow more than 80% confluence, the cells were plated at low density (2×10^4 cells/ cm^2) in a 96-well plate for differentiation into neurons and MTT assay. After 3 days, the medium was replaced with growth medium containing 50 ng/mL neuron growth factor- β (NGF- β , Sigma-Aldrich) and 1.0 μM dexamethasone (Sigma-Aldrich). The cells were differentiated on day 7.

The skeletal muscle cell line (C2C12, ATCC) myoblasts were cultured in a growth medium consisting of Dulbecco's modified Eagle Medium high glucose with L-glutamine and sodium pyruvate (DMEM, Biowest, MA, USA), supplemented with 10% FBS and 1% P/S. Differentiation medium consisted of DMEM supplemented with 10% inactivated donor HS (Biowest) and 1% P/S. Myoblasts differentiated into myotubes on day 7. The cells were maintained at 37 $^{\circ}\text{C}$ in a 95% humidified incubator with 5% CO_2 . The medium was replaced with fresh medium every 2–3 days.

Cell Viability after McMiA Treatment. The cells were proliferated in growth medium and exposed to the pristine ionogel, X-BI, X-BI-GO, and McMiA (1.5 mg) for 3, 5, 24, and 48 h. After incubation with 10% MTT (Sigma-Aldrich) in growth medium at 37 $^{\circ}\text{C}$ and 5% CO_2 for 4 h, a lysis buffer solution [50% (w/v) *N,N*-dimethylformamide (DMF, Sigma-Aldrich) in distilled water and 10% (w/v) sodium dodecyl sulfate (SDS, Sigma-Aldrich)] was added in each well to stop the reaction. The 96-well plates were incubated at room temperature for 2 h for formazan diffusion into the medium in dark. The OD was measured at 570 nm using a microplate reader (Thermo Fisher Scientific).

Physicochemical Characterization of McMiA. The ion diffusion barrier effect of McMiA was evaluated in HDFn cells (Figure S15a). HDFn cells were prepared in a transwell culture system with tissue culture inserts in a 12-well plate (cat no. 665640, Greiner). An electrical stimulation test was designed such that the ionogel for stimulation voltage was closely adhered to the inset membrane, and the growth medium was contained on the cells to form a ground. The electrical stimulation system is a two-electrode system consisting of a working electrode and a counter electrode. The counter electrode (ground) within the culture medium is introduced to ensure the same direction of current as applied during neural stimulation. HDFn cells were electrically stimulated with and without McMiA at 1 V for 20 s and cultured for 72 h after stimulation. HDFn cell culture media was sampled at 12, 24, 48, and 72 h. Type 1 procollagen, a cellular metabolite, was quantified as the degree of stimulation in HDFn cells.

In addition, the effect of electrical stimulation through McMiA was evaluated in neuronal cells. PC12 cells were cultured in a transwell

culture system with tissue culture inserts in 12-well plate for 3 days and differentiated into neuronal cells for 7 days. An electrical stimulation test was designed such that the ionogel for stimulation voltage was closely adhered to the inset membrane, and the differentiation medium was contained on the cells to form a ground. The neuronal cells were electrically stimulated with and without McMiA at 1 V for 20 s and cultured for 72 h after stimulation. Neuronal cell culture media was sampled at 12, 24, 48, and 72 h. Acetylcholine (ACh), a cellular metabolite essential for muscle contraction, was quantified as the degree of stimulation in neuronal cells. The myoblasts were differentiated to myotube during 7 days in the 6-well culture plates, and the myotube was stimulated with ACh and electrical potential. The ACh, which was produced by electrical stimulated neuronal cells by 72 h, in the culture medium were stimulated to myotube. As a control group, myotubes were stimulated using a bare Au electrode with a bipolar electrical amplitude of ± 20 and ± 0.1 V, at a frequency of 1 Hz. However, we observed cell degradation when subjected to prolonged stimulation at a high voltage under these conditions. To address this issue, we adjusted the electrical stimulation method and performed it under pulse conditions to minimize cell degradation. The contractile of the myotubes was imaged by an optical microscope and live cell imaging. For length contraction measurements of intracellular myotube organelles, random coordinate points were identified on each myotube and measured using ImageJ. Outlined myotubes were then exported to ImageJ for the area contraction measurements of myotubes.

Design of Neurostimulator. A neurostimulator consisting of a battery, main board, and wireless power transfer (WPT) antenna for generating stimulation pulses was developed to demonstrate the feasibility of the proposed electrode for neuromodulation. A small, low-power, wireless microcontroller (MCU) supporting BLE CC2640R2F (Texas Instruments, USA) was used for wireless communication and pulse control. The MCU communicates with a smartphone through Bluetooth low energy (BLE) communication to receive commands and can change the output voltage through I2C communication with a DAC MCP4726 (Microchip Technology, USA). The two output terminals connected to the electrodes are connected to the DAC's output and circuit ground. This connection is configured using field effect transistors (FETs) as a switch, allowing the polarity of the pulses to be changed. The main board and WPT antenna include a four-layer printed circuit board (PCB) and use a 13.56 MHz signal for wireless charging. The device was packaged using biocompatible epoxy (EPO-TEK 301, Epoxy Technology, USA).

In Vivo Experiment. All animal experiments were approved by the Institutional Animal Care and Use Committee (IACUC) at Pohang University of Science and Technology (POSTECH) (approval number: POSTECH-2021-0099). A surgery for implanting a neural stimulator device and a surgery for saline injection and bladder pressure measurement were performed. A Sprague–Dawley rat (280 g, 9-week-old male, ORIENT, Korea) was anaesthetized with 2% inhaled isoflurane using a tube. First, after hair removal and an incision in the lower abdomen, the bladder was exposed, a hole was punched in the bladder, and a PE 50 tube (BTPE-50, Instech) was inserted. The tube insertion site was sutured with 4–0 prolene to prevent leakage. The other end of the tube was passed subcutaneously near the neck of the rat and connected to an access button (VABR1B/22, Instech) connected to the fluid rotation system.

Next, hair was removed around the thigh and back of the rat to implant the electrode and nerve-stimulating device. The skin and muscles near the thigh were incised to locate the sciatic nerve and connected to the electrode. The device was placed subcutaneously on the dorsal side, and the electrodes and the device were connected subcutaneously using insulated wires. Using the smartphone app, commands for device manipulation were sent through BLE communication, and a leg trembling confirmed that the nerve stimulation system, including electrodes and devices, worked properly and the sciatic nerve was properly stimulated. After all surgeries were completed, there was a recovery period of 1 day, and a nerve stimulation experiment was performed to confirm the effect of

inhibiting voiding. A rat was placed in a metabolic cage (C-72R-K, degree B&P, member of the National Assembly), the tube was connected to an access button, and then connected to a three-way Y connector (SCY22, Instech) to connect the tube, pressure converter (IX-RA-834, iWorx), and the injection pump. A saline solution (0.9% NaCl) was continuously injected into the bladder with an injection pump (100 $\mu\text{L}/\text{min}$), and the change in bladder pressure was recorded by a pressure converter at 1 Hz sampling rate. The amount of urine accumulated was measured by measuring the weight of urine using an electronic scale connected to a PC. The device can turn on and off the generation of nerve stimulation signals, which are characterized by short (100 μs width) biphasic pulses at the repetition frequency of 10 Hz and amplitude of 1.5 V, using a smartphone app. Urination activity was analyzed by comparing data from 30 min before the signal was turned on (pre) and 30 min after the signal was turned on (post).

ASSOCIATED CONTENT

Supporting Information

The Supporting Information is available free of charge at <https://pubs.acs.org/doi/10.1021/acsnano.3c02637>.

Synthesis and functionalization of McMiA materials Figure S1–S20: synthesis of biocompatible $[\text{Ch}]^+[\text{MA}]^-$ ionic liquid; molecular characterization of X-BI; swelling property of X-BI; Schematic illustration of cross-linking mechanism of X-GO and X-BI; molecular characterization of X-GO; Detachment ratio of pristine GO and dopamine-cross-linked GO (X-GO) layer from the cross-cut test; Impedance change of McMiA soaked in PBS under mechanical stretching (0–30% strain) for 10 h; Strain–stress curves of pristine chitosan polymer film and X-BI films as a function of ionic liquid concentration (10–50 wt %); DSC curves of X-BI films as a function of ionic liquid concentration (10–50 wt %); Normalized time-dependent stress-relaxation behavior of McMiA by soaking in water over time; surface modulus map images of X-BI and McMiA; CV profiles of PBS solution and $[\text{Ch}]^+[\text{MA}]^-$ with scan rate of 5 mV s^{-1} ; Cyclic voltammograms curves for $[\text{Ch}]^+[\text{MA}]^-$ ionic liquids with different water concentration (0–50 v/v%); Impedance spectra of the McMiA after soaking in PBS for 1–8 h; Cytotoxicity characterization of ionogels and McMiA; Differentiation of neuron cells and muscle cells; Electrical stimulation setup, and functional activity of dermal fibroblasts and neuronal cells; Design of wireless neurostimulator; *in vivo* experimental environment setting; *in vivo* experimental environment setting (PDF)

Adhesion test in PBS solution (MP4)

Electrical stimulation with McMiA on myotube (MP4)

Electrical stimulation with McMiA on sciatic nerve and leg tremor response (MP4)

AUTHOR INFORMATION

Corresponding Authors

Do Hwan Kim – Department of Chemical Engineering, Hanyang University, Seoul 04763, Republic of Korea; Institute of Nano Science and Technology and Clean-Energy Research Institute, Hanyang University, Seoul 04763, Republic of Korea; orcid.org/0000-0003-3003-8125; Email: dhkim76@hanyang.ac.kr

Sung-Min Park – School of Interdisciplinary Bioscience and Bioengineering, Pohang University of Science and Technology, Pohang 37673, Republic of Korea; Department of

Convergence IT Engineering, Pohang University of Science and Technology, Pohang 37673, Republic of Korea; Email: sungminpark@postech.ac.kr

Jaе Hyun Jeong – Department of Chemical Engineering, Soongsil University, Seoul 06978, Republic of Korea; Email: nfejhh@ssu.ac.kr

Authors

Joo Sung Kim – Department of Chemical Engineering, Hanyang University, Seoul 04763, Republic of Korea

Junho Kim – School of Interdisciplinary Bioscience and Bioengineering, Pohang University of Science and Technology, Pohang 37673, Republic of Korea

Jun Woo Lim – Department of Chemical Engineering, Soongsil University, Seoul 06978, Republic of Korea

Dong Jun Kim – Department of Chemical Engineering, Hanyang University, Seoul 04763, Republic of Korea

Jong Ik Lee – Department of Chemical and Biomolecular Engineering, Sogang University, Seoul 04107, Republic of Korea

Hanbin Choi – Department of Chemical Engineering, Hanyang University, Seoul 04763, Republic of Korea

Hyukmin Kweon – Department of Chemical Engineering, Hanyang University, Seoul 04763, Republic of Korea

Jiho Lee – Department of Convergence IT Engineering, Pohang University of Science and Technology, Pohang 37673, Republic of Korea

Hyeono Yee – Department of Chemical and Biomolecular Engineering, Sogang University, Seoul 04107, Republic of Korea

Ji Hong Kim – Department of Chemical Engineering, Hanyang University, Seoul 04763, Republic of Korea

Bokyung Kim – Department of Chemical Engineering, Hanyang University, Seoul 04763, Republic of Korea

Moon Sung Kang – Department of Chemical and Biomolecular Engineering, Sogang University, Seoul 04107, Republic of Korea; Institute of Emergent Materials, Sogang University, Seoul 04107, Republic of Korea

Complete contact information is available at:

<https://pubs.acs.org/doi/10.1021/acsnano.3c02637>

Author Contributions

J.S.K., J.K., and J.W.L. contributed equally to this work. J.H.J., S.-M.P., and D.H.K. supervised the project. J.S.K. and D.H.K. conceived the concept. J.S.K., J.K., and J.W.L. designed and carried out experiments. J.S.K., D.J.K., J.H.K., and B.K. synthesized the McMiA and fabricated the devices. J.K., J.L., and S.-M.P. designed and conducted the *in vivo* animal experiments. J.S.K., H.C., and H.K. conducted the mechanical characterizations of the McMiA. J.W.L. and J.H.J. designed and conducted physiochemical characterization of McMiA. J.S.K., J.I.L., H.Y., and M.S.K. designed and conducted electrochemical characterizations of the choline malate ionic liquid and McMiA. J.S.K., J.K., J.W.L., J.H.J., S.-M.P., and D.H.K. wrote the manuscript. All authors reviewed and commented on the manuscript.

Notes

The authors declare no competing financial interest.

ACKNOWLEDGMENTS

This work was supported by the National R&D Program (2021M3H4A1A03049075) and Basic Science Research

Program (2017R1A5A1015596, 2020R1A6A1A03044977) through the National Research Foundation of Korea (NRF) funded by the Ministry of Science, ICT, and Education, Republic of Korea.

REFERENCES

- (1) Guyot, M.; Simon, T.; Ceppo, F.; Panzolini, C.; Guyon, A.; Lavergne, J.; Murriss, E.; Daoudliarian, D.; Brusini, R.; Zarif, H.; Abelanet, S.; Hugues-Ascery, S.; Divoux, J.-L.; Lewis, S. J.; Sridhar, A.; Glaichenhaus, N.; Blancou, P. Pancreatic nerve electrostimulation inhibits recent-onset autoimmune diabetes. *Nat. Biotechnol.* **2019**, *37*, 1446–1451.
- (2) Johnson, R. L.; Wilson, C. G. A review of vagus nerve stimulation as a therapeutic intervention. *J. Inflamm. Res.* **2018**, *11*, 203.
- (3) Lai, H. Y.; Liao, L. D.; Lin, C. T.; Hsu, J. H.; He, X.; Chen, Y. Y.; Chang, J. Y.; Chen, H. F.; Tsang, S.; Shih, Y. Y. I. Design, simulation and experimental validation of a novel flexible neural probe for deep brain stimulation and multichannel recording. *J. Neural Eng.* **2012**, *9*, 036001.
- (4) Jun, J. J.; Steinmetz, N. A.; Siegle, J. H.; Denman, D. J.; Bauza, M.; Barbarits, B.; Lee, A. K.; Anastassiou, C. A.; Andrei, A.; Aydın, C.; Barbic, M.; Blanche, T. J.; Bonin, V.; Couto, J.; Dutta, B.; Gratiy, S. L.; Gutnisky, D. A.; Häusser, M.; Karsh, B.; Ledochowitsch, P.; Lopez, C. M.; Mitelut, C.; Musa, S.; Okun, M.; Pachitariu, M.; Putzeys, J.; Rich, P. D.; Rossant, C.; Sun, W. L.; Svoboda, K.; Carandini, M.; Harris, K. D.; Koch, C.; O'Keefe, J.; Harris, T. D. Fully integrated silicon probes for high-density recording of neural activity. *Nature* **2017**, *551*, 232–236.
- (5) Rejc, E.; Angeli, C. A.; Atkinson, D.; Harkema, S. J. Motor recovery after activity-based training with spinal cord epidural stimulation in a chronic motor complete paraplegic. *Sci. Rep.* **2017**, *7*, 1–12.
- (6) Rowald, A.; Komi, S.; Demesmaeker, R.; Baaklini, E.; Hernandez-Charpak, S. D.; Paoles, E.; Montanaro, H.; Cassara, A.; Becce, F.; Lloyd, B.; Newton, T.; Ravier, J.; Kinany, N.; D'Ercole, M.; Paley, A.; Hankov, N.; Varescon, C.; McCracken, L.; Vat, M.; Caban, M.; Watrin, A.; Jacquet, C.; Bole-Feysot, L.; Harte, C.; Lorach, H.; Galvez, A.; Tschopp, M.; Herrmann, N.; Wacker, M.; Geernaert, L.; Fodor, I.; Radevich, V.; Van Den Keybus, K.; Eberle, G.; Pralong, E.; Roulet, M.; Ledoux, J.-B.; Fornari, E.; Mandija, S.; Mattera, L.; Martuzzi, R.; Nazarian, B.; Benkler, S.; Callegari, S.; Greiner, N.; Fuhrer, B.; Froeling, M.; Buse, N.; Denison, T.; Buschman, R.; Wende, C.; Ganty, D.; Bakker, J.; Delattre, V.; Lambert, H.; Minassian, K.; van den Berg, C. A. T.; Kavounoudias, A.; Micera, S.; Van De Ville, D.; Barraud, Q.; Kurt, E.; Kuster, N.; Neufeld, E.; Capogrosso, M.; Asboth, L.; Wagner, F. B.; Bloch, J.; Courtine, G. Activity-dependent spinal cord neuromodulation rapidly restores trunk and leg motor functions after complete paralysis. *Nat. Med.* **2022**, *28*, 260–271.
- (7) Yao, G.; Kang, L.; Li, J.; Long, Y.; Wei, H.; Ferreira, C. A.; Jeffery, J. J.; Lin, Y.; Cai, W.; Wang, X. Effective weight control via an implanted self-powered vagus nerve stimulation device. *Nat. Commun.* **2018**, *9*, 1–10.
- (8) de Groat, W. C.; Tai, C. Mechanisms of action of sacral nerve and peripheral nerve stimulation for disorders of the bladder and bowel. *Neuromodulation: comprehensive textbook of principles, technologies, and therapies*; Elsevier: Cambridge, UK, 2018.
- (9) Kovacevic, M.; Yoo, P. B. Reflex neuromodulation of bladder function elicited by posterior tibial nerve stimulation in anesthetized rats. *Am. J. Physiol. Renal Physiol.* **2015**, *308*, F320–F329.
- (10) Magissetty, R. P.; Park, S. M. New Era of Electroceuticals: Clinically Driven Smart Implantable Electronic Devices Moving towards Precision Therapy. *Micromachines* **2022**, *13*, 161.
- (11) Mickle, A. D.; Won, S. M.; Noh, K. N.; Yoon, J.; Meacham, K. W.; Xue, Y.; McIlvried, L. A.; Copits, B. A.; Samineni, V. K.; Crawford, K. E.; Kim, D. H.; Srivastava, P.; Kim, B. H.; Min, S.; Shiuan, Y.; Yun, Y.; Payne, M. A.; Zhang, J.; Jang, H.; Li, Y.; Lai, H. H.; Huang, Y.; Park, S. I.; Gereau, R. W., IV; Rogers, J. A. A wireless closed-loop system for optogenetic peripheral neuromodulation. *Nature* **2019**, *565*, 361–365.
- (12) Zhang, Y.; Mickle, A. D.; Gutruf, P.; McIlvried, L. A.; Guo, H.; Wu, Y.; Golden, J. P.; Xue, Y.; Grajales-Reyes, J. G.; Wang, X.; Krishnan, S.; Xie, Y.; Peng, D.; Su, C. J.; Zhang, F.; Reeder, J. T.; Vogt, S. K.; Huang, Y.; Rogers, J. A.; Gereau, R. W., IV Battery-free, fully implantable optofluidic cuff system for wireless optogenetic and pharmacological neuromodulation of peripheral nerves. *Sci. Adv.* **2019**, *5*, No. eaaw5296.
- (13) Čvančara, P.; Boretius, T.; López-Álvarez, V. M.; Maciejasz, P.; Andreu, D.; Raspopovic, S.; Petrini, F.; Micera, S.; Granata, G.; Fernandez, E.; Rossini, P. M.; Yoshida, K.; Jensen, W.; Divoux, J. L.; Guiraud, D.; Navarro, X.; Stieglitz, T. Stability of flexible thin-film metallization stimulation electrodes: analysis of explants after first-in-human study and improvement of in vivo performance. *J. Neural Eng.* **2020**, *17*, 046006.
- (14) Sikder, K. U.; Shivdasani, M. N.; Fallon, J. B.; Seligman, P.; Ganesan, K.; Villalobos, J.; Prawer, S.; Garrett, D. J. Electrically conducting diamond films grown on platinum foil for neural stimulation. *J. Neural Eng.* **2019**, *16*, 066002.
- (15) Nguyen, J. K.; Park, D. J.; Skousen, J. L.; Hess-Dunning, A. E.; Tyler, D. J.; Rowan, S. J.; Weder, C.; Capadona, J. R. Mechanically-compliant intracortical implants reduce the neuroinflammatory response. *J. Neural Eng.* **2014**, *11*, 056014.
- (16) Lee, S. H.; Ozlu, B.; Eom, T.; Martin, D. C.; Shim, B. S. Electrically conducting polymers for bio-interfacing electronics: From neural and cardiac interfaces to bone and artificial tissue biomaterials. *Biosens. Bioelectron.* **2020**, *170*, 112620.
- (17) Liu, Y.; Liu, J.; Chen, S.; Lei, T.; Kim, Y.; Niu, S.; Wang, H.; Wang, X.; Foudeh, A. M.; Tok, J. B. H.; Bao, Z. Soft and elastic hydrogel-based microelectronics for localized low-voltage neuro-modulation. *Nat. Biomed. Eng.* **2019**, *3*, 58–68.
- (18) Liu, Y.; Li, J.; Song, S.; Kang, J.; Tsao, Y.; Chen, S.; Mottini, V.; McConnell, K.; Xu, W.; Zheng, Y.-Q.; Tok, J. B.-H.; George, P. M.; Bao, Z. Morphing electronics enable neuromodulation in growing tissue. *Nat. Biotechnol.* **2020**, *38*, 1031–1036.
- (19) Zhao, S.; Tseng, P.; Grasman, J.; Wang, Y.; Li, W.; Napier, B.; Yavuz, B.; Chen, Y.; Howell, L.; Rincon, J.; Omenetto, F. G.; Kaplan, D. L. Programmable hydrogel ionic circuits for biologically matched electronic interfaces. *Adv. Mater.* **2018**, *30*, 1800598.
- (20) Mochizuki, Y.; Horii, T.; Okuzaki, H. Effect of pH on structure and conductivity of PEDOT/PSS. *Trans. Mater. Res. Soc. Jpn.* **2012**, *37*, 307–310.
- (21) Deng, J.; Yuk, H.; Wu, J.; Varela, C. E.; Chen, X.; Roche, E. T.; Guo, C. F.; Zhao, X. Electrical bioadhesive interface for bioelectronics. *Nat. Mater.* **2021**, *20*, 229–236.
- (22) Hejazi, M.; Tong, W.; Ibbotson, M. R.; Prawer, S.; Garrett, D. J. Advances in carbon-based microfiber electrodes for neural interfacing. *Front. Neurosci.* **2021**, *15*, 658703.
- (23) Cogan, S. F. Neural stimulation and recording electrodes. *Annu. Rev. Biomed. Eng.* **2008**, *10*, 275–309.
- (24) Alimohamadi, M.; Saghafeina, M.; Alikhani, F.; Danial, Z.; Shirani, M.; Amirjamshidi, A. Impact of electrolyte imbalances on the outcome of aneurysmal subarachnoid hemorrhage: A prospective study. *Asian J. Neurosurg.* **2016**, *11*, 29.
- (25) Li, X.; Ma, N.; Zhang, L.; Ling, G.; Zhang, P. Applications of choline-based ionic liquids in drug delivery. *Int. J. Pharm.* **2022**, *612*, 121366.
- (26) Zhang, M.; Mao, Y.; Liu, G.; Liu, G.; Fan, Y.; Jin, W. Molecular bridges stabilize graphene oxide membranes in water. *Angew. Chem.* **2020**, *132*, 1706–1712.
- (27) Mi, F. L.; Tan, Y. C.; Liang, H. F.; Sung, H. W. In vivo biocompatibility and degradability of a novel injectable-chitosan-based implant. *Biomaterials* **2002**, *23*, 181–191.
- (28) Pandey, N.; Soto-Garcia, L.; Yaman, S.; Kuriakose, A.; Rivera, A. U.; Jones, V.; Liao, J.; Zimmern, P.; Nguyen, K. T.; Hong, Y. Polydopamine nanoparticles and hyaluronic acid hydrogels for

mussel-inspired tissue adhesive nanocomposites. *Biomaterials Advances* **2022**, *134*, 112589.

(29) Yuk, H.; Lu, B.; Zhao, X. Hydrogel bioelectronics. *Chem. Soc. Rev.* **2019**, *48*, 1642–1667.

(30) Ravagli, E.; Mastitskaya, S.; Thompson, N.; Iacoviello, F.; Shearing, P. R.; Perkins, J.; Gourine, A. V.; Aristovich, K.; Holder, D. Imaging fascicular organization of rat sciatic nerves with fast neural electrical impedance tomography. *Nat. Commun.* **2020**, *11*, 1–10.

(31) Lee, J. I.; Choi, H.; Kong, S. H.; Park, S.; Park, D.; Kim, J. S.; Kwon, S. H.; Kim, J.; Choi, S. H.; Lee, S. G.; Kim, D. H.; Kang, M. S. Visco-Poroelastic Electrochemiluminescence Skin with Piezo-Ionic Effect. *Adv. Mater.* **2021**, *33*, 2100321.

(32) Tomiyasu, H.; Shikata, H.; Takao, K.; Asanuma, N.; Taruta, S.; Park, Y. Y. An aqueous electrolyte of the widest potential window and its superior capability for capacitors. *Sci. Rep.* **2017**, *7* (1), 1–12.

(33) Chen, M.; Wu, J.; Ye, T.; Ye, J.; Zhao, C.; Bi, S.; Yan, J.; Mao, B.; Feng, G. Adding salt to expand voltage window of humid ionic liquids. *Nat. Commun.* **2020**, *11* (1), 5809.

(34) Bi, S.; Wang, R.; Liu, S.; Yan, J.; Mao, B.; Kornyshev, A. A.; Feng, G. Minimizing the electrosorption of water from humid ionic liquids on electrodes. *Nat. Commun.* **2018**, *9* (1), 5222.

(35) Weltin, A.; Kieninger, J. Electrochemical methods for neural interface electrodes. *J. Neural Eng.* **2021**, *18*, 052001.

(36) Zhou, D. D.; Cui, X. T.; Hines, A.; Greenberg, R. J. Techniques and Engineering Approaches. In *Implantable Neural Prostheses*; Zhou, D. D., Greenbaum, E., Eds.; Springer, 2010; Vol. 2.

(37) Gad, P.; Choe, J.; Nandra, M. S.; Zhong, H.; Roy, R. R.; Tai, Y. C.; Edgerton, V. R. Development of a multi-electrode array for spinal cord epidural stimulation to facilitate stepping and standing after a complete spinal cord injury in adult rats. *J. Neuroeng. Rehabilitation* **2013**, *10*, 1–18.

(38) Schiavone, G.; Fallegger, F.; Kang, X.; Barra, B.; Vachicouras, N.; Roussinova, E.; Furfaro, I.; Jiguet, S.; Seáñez, I.; Borgognon, S.; Rowald, A.; Li, Q.; Qin, C.; Bézard, E.; Bloch, J.; Courtine, G.; Capogrosso, M.; Lacour, S. P. Soft, Implantable Bioelectronic Interfaces for Translational Research. *Adv. Mater.* **2020**, *32*, 1906512.

(39) Koopman, F. A.; Schuurman, P. R.; Vervoordeldonk, M. J.; Tak, P. P. Vagus nerve stimulation: a new bioelectronics approach to treat rheumatoid arthritis? *Best practice & research Clinical rheumatology* **2014**, *28* (4), 625–635.

(40) de Wall, L. L.; Heesakkers, J. P. Effectiveness of percutaneous tibial nerve stimulation in the treatment of overactive bladder syndrome. *Res. Rep. Urol.* **2017**, *9*, 145.

(41) de Groat, W. C.; Yoshimura, N. A. O. K. I. Anatomy and physiology of the lower urinary tract. *Handb. Clin. Neurol.* **2015**, *130*, 61–108.

(42) Simillis, C.; Lal, N.; Qiu, S.; Kontovounisios, C.; Rasheed, S.; Tan, E.; Tekkis, P. P. Sacral nerve stimulation versus percutaneous tibial nerve stimulation for faecal incontinence: a systematic review and meta-analysis. *Int. J. Colorectal Dis.* **2018**, *33*, 645–648.

(43) Zeiton, M.; Faily, S.; Nicholson, J.; Telford, K.; Sharma, A. Sacral nerve stimulation—hidden costs (uncovered). *Int. J. Colorectal Dis.* **2016**, *31*, 1005–1010.

(44) Abello, A.; Das, A. K. Electrical neuromodulation in the management of lower urinary tract dysfunction: evidence, experience and future prospects. *Ther. Adv. Urol.* **2018**, *10*, 165–173.

(45) Hultén, L.; Angerås, U.; Scaglia, M.; Delbro, D. Sacral nerve stimulation (SNS), posterior tibial nerve stimulation (PTNS) or acupuncture for the treatment for fecal incontinence: a clinical commentary. *Technol. Coloproctol.* **2013**, *17*, 589–592.

(46) Bhidé, A. A.; Tailor, V.; Fernando, R.; Khullar, V.; Digesu, G. A. Posterior tibial nerve stimulation for overactive bladder—techniques and efficacy. *Int. Urogynecol. J.* **2020**, *31*, 865–870.

The advertisement features a vertical image on the left showing a blue, translucent, spherical object with a yellow, textured, tube-like structure extending from its base, which is surrounded by a cluster of green and yellow spheres. The background is a dark blue gradient. Text is overlaid on the right side in white and yellow.

CAS BIOFINDER DISCOVERY PLATFORM™

**PRECISION DATA
FOR FASTER
DRUG
DISCOVERY**

CAS BioFinder helps you identify
targets, biomarkers, and pathways

Unlock insights

CAS
A division of the
American Chemical Society